Prepared Under The Joint Sponsorship
of The U. S. Air Force Project RAND
and
Subcontract SC-9 With The
Los Alamos Scientific Laboratory

RESEARCH MEMORANDUM

NUMERICAL SOLUTIONS OF SPHERICAL BLAST WAVES

H. L. Brode

RM-1363-AEC

29 September 1954

Assigned to _____

This is a working paper. It may be expanded, modified, or withdrawn at any time.

The RAND Corporation
1700 MAIN ST. • SANTA MONICA • CALIFORNIA

NUMERICAL SOLUTIONS OF SPHERICAL BLAST WAVES

Harold L. Brode
The RAND Corporation, Santa Monica, California

ABSTRACT

The strong-shock, point-source solution and spherical isothermal distributions were used as initial conditions for a numerical integration of the differential equations of gas motion in Lagrangean form. The Von Neumann-Richtmyer artificial viscosity was employed to avoid shock discontinuities. The solutions were carried from two thousand atmospheres to less than one-tenth atmospheres peak overpressure. Results include overpressure, density, particle velocity, and position as functions of time and space. The dynamic pressure, the positive and negative impulses of both dynamic pressure and static overpressure, positive and negative durations of pressure and velocity, and shock values of all quantities are also described for various times and radial distances. Analytical approximations to the numerical results are provided.

I. INTRODUCTION

The problem of a spherical blast in air has been solved analytically for strong shocks in an ideal gas by J. von Neumann[1], and in the weak shock approximation by H. A. Bethe[1]. For intermediate regions it has been found necessary to resort to numerical methods. The availability of high speed computing machines has made possible the solution of this problem in the intermediate range with considerable accuracy.

Two other groups are currently engaged in performing this work by independent methods. Under J. Von Neumann and H. Goldstine at Princeton a shock fitting method has been employed. The differencing method of Peter Lax[2] is being used at New York University by S. Lowell.

The method used in this paper is due to von Neumann and Richtmyer[3] and employs an artificial viscosity as a mechanism for avoiding shock-front discontinuities. Previously T. S. Walton reported some results[4] using this method and an initial isobaric sphere of about 13 atmospheres.

The integrating process consists of the step-wise solution of difference equations which approximate the differential equations of motion of the gas. In order for such a procedure to be workable, however, a number of practical conditions must be satisfied. The differencing scheme must be stable, must offer reasonably detailed results, must conserve numerical significance, and when put in the form of coded instructions for a high-speed computer, must be fast enough to reach desired solutions with a reasonable expenditure of machine time.

In addition, scaling problems arise from the wide range of numerical values that must be accommodated. Furthermore, the continual increase of shock radius requires some recurring adjustments in zone number and sizes to preserve a maximum amount of information in a limited number of zones. In the end, several compromises must be worked between such conflicting requirements as the need for frequent printed or card-punched records of the progress of the problem and a desire to minimize the machine time involved in printing or punching. Similarly, the desire for small zones, sharp shock fronts and smooth results is inconsistent with the need for large time steps and limited space points. For simplicity, these first problems were done with an homogeneous ideal gas (constant specific heat ratio, $\gamma = 1.4$), and for the simple initial conditions of either the strong shock point source solution[1] or an isothermal sphere.

II. METHOD FOR NUMERICAL INTEGRATION

EQUATIONS OF MOTION

The Lagrangean equations of motion are reduced to dimensionless parameters wherein pressure (P), density (ρ), and velocity (u) are measured in units of ambient pressure (P_o), density (ρ_o), and sound velocity (C_o), respectively. In the following discussion, the pressure will frequently be expressed in atmospheres where one atmosphere is defined as equal to the pre-shock ambient pressure (P_o). Where the expression overpressure (ΔP) is used the reference is to the pressure in atmospheres in excess of the ambient pressure (P_o), i.e., $\Delta P = P-1$. We shall continue to speak of a velocity (u), however, when more properly we might refer to a mesh number (u). The radial distance $r(r_o,t)$, is expressed in energy-reduced dimensionless units (r_o being Lagrangean distance, and t the time), such that

$$\lambda = r/\epsilon \text{ and } \lambda_o = r_o/\epsilon \ , \tag{1}$$

where ϵ is a length expressing the energy and ambient pressure scaling:

$$\epsilon^3 = \frac{E_{tot}}{P_o} = \frac{4\pi}{P_o} \int_o^R \rho\left(E_{int} + \frac{u^2}{2}\right) r^2 \, dr - \frac{4\pi R^3}{3(\gamma-1)} \ . \tag{2}$$

E_{tot} is the total blast energy and E_{int} is the specific internal energy. The subtracted term represents the pre-shock internal energy of the gas engulfed by the shock, and R is the shock radius. Time (t) is defined in dimensionless units (τ) such that

$$\tau = t\, c_o/\epsilon \ .$$

The artificial viscosity (q), which acts like a pressure, is in units of the pre-shock ambient pressure (P_o).

In these units the Lagrangean equations of motion are written as follows:

$$\frac{\partial \lambda}{\partial x} = \frac{1}{\rho \lambda^2} \text{ or } \frac{\partial \rho}{\partial \tau} = -\rho\left(\frac{2u}{\lambda} + \frac{\partial u/\partial x}{\partial \lambda/\partial x}\right) \quad \text{(mass)} , \tag{3}$$

$$\frac{\partial u}{\partial \tau} = \frac{\lambda^2}{\gamma} \frac{\partial}{\partial x} (P + q) \quad \text{(momentum)} , \tag{4}$$

$$\frac{\partial P}{\partial \tau} = \frac{1}{\rho} \frac{\partial \rho}{\partial \tau} \left[\gamma P + (\gamma - 1)\, q\right] \quad \text{(energy)} , \tag{5}$$

$$u = \frac{\partial \lambda}{\partial \tau} . \tag{6}$$

In these equations the Lagrangean variable is taken to be $x = 1/3\ (r_o/\epsilon)^3$.

In Eq. 5 (energy conservation) the internal energy for an ideal gas has been used.

$$E = \frac{P}{\rho(\gamma-1)} \frac{\rho_o}{P_o} \tag{7}$$

FORM OF ARTIFICIAL VISCOSITY

An appropriate viscosity for the case of an outward moving spherical shock wave is the following:

$$q = \frac{9\gamma(\gamma+1)}{4} \left(\frac{M}{3x}\right)^2 \rho(\Delta x)^2 \left(\frac{\partial u}{\partial x}\right) \left(\frac{\partial u}{\partial x} - \left|\frac{\partial u}{\partial x}\right|\right) \tag{8}$$

where Δx is the grid size and M is the number of grid zones in the shock front. The form of q chosen here is basically similar to that of von Neumann and Richtmyer, and satisfies similar conditions for the spherical case. However, there is no convenient steady-state solution by which to demonstrate the connection of variables across the shock, and the form chosen here is only asymptotically the same as a verified form for a plane problem.

The fact that the plane form approximation is good for shock thicknesses which are small relative to the shock radius is borne out by the close agreement with a similarity solution (with q) investigated by R. Latter[5] in which he solves numerically the resulting ordinary differential equations for cases of interest to this problem.

The particular form chosen for the viscosity has the advantage that it contributes nothing in regions of expansion, and is non-zero only in the compression phase of a shock. In Lagrangean coordinates this has the advantage of eliminating a spurious contribution near the origin where the positive velocity gradient is large.

The artificial viscosity, being essentially a diffusive mechanism, may force one to use excessively small time increments in order to achieve smooth results on a fine space grid.

INITIAL CONDITIONS

Two general types of initial conditions were taken, (1) a point-source, and (2) an isothermal sphere. A point-source case was run in the greatest length using the von Neumann strong-shock solution beginning at 1600 atmos shock overpressure, and running down to less than 0.06 atmos. The point-source solution, starting at 199 atmos peak overpressure, was used to start the one problem carried out on the ORDVAC machine at the Ballistics Research Laboratories, Aberdeen, Maryland. The latter problem was run to nearly 0.1 atmos shock overpressure. The point-source solution was also used for starts at 473 and 818 atmos shock overpressure, and these problems were run down to less than 100 atmos peak overpressure.

Three isothermal-sphere type problems have been run so far. Two of these begin with a hot isothermal sphere for which the density is the same inside and out. One began at 2002 atmos, the other at 121 atmos, overpressure.

One cold isothermal sphere was also used, beginning with 121 atmos overpressure and a temperature inside equal to the outside temperature.

These three problems were carried down to shock overpressures less than unity.

Numerous shorter problems were also run, principally for the sake of empirical checks on computational methods, or in amplification of special features of the previously mentioned problems.

Short plane-geometry problems were found useful in checking the validity of various computational tricks, and in studying the effect of certain changes in the difference equations. The effect of the size of the viscosity constant was also more easily studied in the plane case. Time increments smaller than that prescribed by the Courant Condition ($\Delta\tau = (p\rho)^{-\frac{1}{2}}\Delta r$) by a factor of 2 to 4 were found necessary for smooth results. In an attempt to reduce the required computing time the stable differencing scheme of Du Fort and Frankel[6] for diffusion-type equations was employed in place of explicitly carrying a viscosity quantity (q). Unfortunately such a scheme has some practical disadvantages. It requires carrying throughout a machine calculation sets of data for all space points for two different times. Furthermore, computing, changing time increments, and combining space points all become more tedious. Besides these disadvantages, additional terms must be introduced to correct for the excess energy introduced by the differencing scheme. On the other hand, the very general nature of the viscosity method, the ease of its applicability, and the precision with which it reproduces the Hugoniot conditions across a shock would seem to offset the more stringent time requirement. Use of this method for non-ideal gases is not considered in this paper, however.

It is frequently convenient to use unequal zone sizes. For instance, the use of small zones through the shock front provides a sharp shock at very little cost in computing time. The use of such unequal zones was empirically validated in this problem by repeating calculations with quite different zone choices.

The size of the time increments were automatically doubled whenever the stability conditions would allow it. Two conditions exist, one being the usual Courant Condition and the other a diffusion-type condition imposed by the artificial viscosity

$$\Delta\tau \leq \Delta x/\lambda^2 \, (p\rho)^{\frac{1}{2}}_{max}$$

$$\Delta\tau \leq \frac{\gamma}{4} (\Delta x)^2 \left[\frac{1}{\lambda^2 q} \left| \frac{\partial u}{\partial x} \right| \right]_{min} . \qquad (9)$$

The total energy in the blast wave must be conserved, but a check on the total energy is not a very sensitive test of the correctness of the results. Several machine errors were detected (and eliminated) which did not substantially effect the total energy. The most reliable check seems to be to re-run a problem with minor alterations. Such a re-run not only catches machine errors but serves to measure the loss of significance. Unfortunately this procedure is costly of machine time, and a compromise might be arranged whereby the machine is instructed to double compute and check itself every cycle. Double computing cannot eliminate errors in storing or transferring, however, and on the particular problem reported here the system employed was to back off and re-run wherever suspicious aberrations occurred and to re-run and compare the entire problem with a different zone spacing, different viscosity, different time increments, as well as some differences in the difference equations.

DIFFERENCE EQUATIONS

The differential equations are approximated by the following difference equations:

$$u_l^{n+\frac{1}{2}} = u_l^{n-\frac{1}{2}} - \frac{\Delta\tau(\lambda^2_l)^2}{(\Delta x)_l \, \gamma} \left[P^n_{l+\frac{1}{2}} - P^n_{l-\frac{1}{2}} + q^{n-\frac{1}{2}}_{l+\frac{1}{2}} - q^{n-\frac{1}{2}}_{l-\frac{1}{2}} \right], \qquad (10)$$

$$\lambda_l^{n+1} = \lambda_l^n + u_l^{n+\frac{1}{2}} \Delta\tau \ , \tag{11}$$

$$W = \Delta\tau \left(\frac{2(u_l^{n+\frac{1}{2}} + u_{l-1}^{n+\frac{1}{2}})}{\lambda_l^{n+1} + \lambda_l^n + \lambda_{l-1}^{n+1} + \lambda_{l-1}^n} + \frac{u_l^{n+\frac{1}{2}} - u_{l-1}^{n+\frac{1}{2}}}{\lambda_l^{n+1} + \lambda_l^n - \lambda_{l-1}^{n+1} - \lambda_{l-1}^n} \right), \tag{12}$$

$$\rho_{l-\frac{1}{2}}^{n+1} = \rho_{l-\frac{1}{2}}^n \left(\frac{1 - W}{1 + W} \right) \ , \tag{13}$$

$$q_{l-\frac{1}{2}}^{n+\frac{1}{2}} = 9 \frac{\gamma(\gamma+1)}{2} \left(\frac{M}{3\pi} \right)^3 \rho_{l-\frac{1}{2}}^{n+1} \left[u_{l-1}^{n+\frac{1}{2}} - u_l^{n+\frac{1}{2}} \right]^2 \ ,$$

$$\text{for } u_{l-1}^{n+\frac{1}{2}} > u_l^{n+\frac{1}{2}}, \tag{14}$$

$$q_{l-\frac{1}{2}}^{n+\frac{1}{2}} = 0 \qquad \text{for } u_{l-1}^{n+\frac{1}{2}} \leqslant u_l^{n+\frac{1}{2}} \ ,$$

$$P_{l-\frac{1}{2}}^{n+1} = \frac{\left[\frac{\gamma+1}{\gamma-1} \rho_{l-\frac{1}{2}}^{n+1} - \rho_{l-\frac{1}{2}}^n \right] P_{l-\frac{1}{2}}^n + 2(\rho_{l-\frac{1}{2}}^{n+1} - \rho_{l-\frac{1}{2}}^n) \, q_{l-\frac{1}{2}}^{n+\frac{1}{2}}}{\frac{(\gamma+1)}{(\gamma-1)} \rho_{l-\frac{1}{2}}^n - \rho_{l-\frac{1}{2}}^{n+1}} \ . \tag{15}$$

III. RESULTS OF NUMERICAL SOLUTIONS

PEAK OVERPRESSURE (P_s) VERSUS SHOCK RADIUS (λ_s)

The strong-shock point-source solution provides that the shock overpressure (ΔP_s) should depend on the inverse cube of the shock radius (λ_s). The problems that were begun with strong-shock, point-source values continued to obey the inverse cube law down to 10 atmos at which point the overpressure had become 3 percent higher than the strong shock prediction. The addition of 1 atmos to an inverse cube term gives a relation valid over a greater range of overpressures, deviating from the calculated curve by less than 5 percent at 5 atmos.

$$\Delta P_s = 0.1567\ \lambda_s^{-3} + 1 \text{ atmos} \qquad (16)$$

The shock radius (λ_s) is in the dimensionless units (energy/pressure-reduced) described in Section II.

At still lower pressures the following empirical fit applies.

$$\Delta P_s = \frac{0.137}{\lambda_s^3} + \frac{0.119}{\lambda_s^2} + \frac{0.269}{\lambda_s} - 0.019 \text{ atmos}\ , \qquad (17)$$

$$\text{for } 0.1 < \Delta P_s < 10, \text{ or } 0.26 < \lambda_s < 2.8\ .$$

For all the calculations begun with a strong-shock the solid curve in Fig. 1 presents the peak overpressure as a function of shock radius.

The dashed curves represent the peak overpressures resulting from the hot isothermal spheres with normal density inside (beginning at 2002 and 122 atmos overpressure). Notice that the overpressure becomes indistinguishable from that of the strong shock at a radius where the mass of air engulfed by the shock is 10 times the initial mass. In the strong shock region this corresponds to a drop in overpressure to about 17 percent of the initial value, and in any case to a radius a little more than twice the initial radius.

The dotted curve represents the overpressure from an initially cold isothermal sphere (normal temperature, high pressure). Because of the slower rarefaction speed the shock pressure does not rise to the point-source value until quite late, i.e., until the rarefaction which moves inward from the initial pressure front has reached the center.

In each case of an initial isothermal sphere there are some slight oscillations about the point source overpressure curve which are caused both by rarefactions and small shocks which form behind the front shock, move inward and reflect off the origin and then move out to overtake the shock front. (See a later discussion of these special features of the sphere problems.)

PEAK DYNAMIC PRESSURE (Q_s) AND PEAK PARTICLE VELOCITY (u_s) VERSUS SHOCK RADIUS (λ_s)

The particle velocity and the peak pressure at the shock front follow precisely the Hugoniot relation,

$$u_s = \frac{5\Delta P_s}{\sqrt{49 + 42\Delta P_s}} . \tag{18}$$

The particle velocity follows its strong-shock dependence on shock radius down to as low an overpressure as 1/10 atmos (Fig. 2); in fact an adequate fit over the entire range is given by the following:

$$u_s = 0.30\, \lambda_s^{-3/2} . \tag{19}$$

This simple form is reflected in the peak dynamic pressure ($Q_s = 1/2\, \rho_s\, u_s^2$) which falls somewhat faster than an inverse cube law down to equally low shock pressures (Fig. 3). The slow decrease in shock density (from 6 for strong shocks to one for weak shocks) is responsible for the decay being steeper than the inverse cube of the shock radius.

PRESSURE (P) VERSUS LAGRANGEAN DISTANCE (R_o)

The pressure behind the shock wave, shown in Fig. 4 as a function of the Lagrangean (or initial position) variable, retains the strong-shock form until quite low pressures. Note, for example, that the ratio of central pressure to shock pressure remains 37 percent down to 20 atmos and decreases slowly below that to 33 percent by 3 atmos. Beyond 3 atmos a negative phase develops with the pressure falling to as low as 0.8 atmos near the center.

In Fig. 4 the Lagrangean position is given in arbitrary units (R_o), related to the dimensionless unit (λ_o) by a constant multiplier,

$$r_o = e\lambda_o = e\frac{R_o}{1627.2} . \qquad (20)$$

It may help in visualizing dimensions to assume R_o to be in centimeters; then the corresponding blast energy will be about that of 200 lbs. of TNT (4.2×10^{15} ergs).

PARTICLE VELOCITY (u) AND DENSITY (ρ) VERSUS LAGRANGEAN DISTANCE (R_o)

Figs. 5 and 6 indicate the progression of particle velocity and density as functions of the Lagrangean position. Again the strong-shock form is dominant until as low as 3 atmos of shock overpressure.

The particle velocity transforms gradually from its very linear form to one much like the overpressure at large distances as the shock wave goes from strong to weak.

The density, which in the strong shock is zero at the origin, implying an infinite temperature, remains zero there since no mechanism is included (no conduction or radiation) for dissipating this high temperature.

The density profiles in Fig. 6 represent strong shock initial conditions at 200 atmos shock pressure. The dip in the curves that sit at the same mass point ($R_o = 150$) is due to the sudden inclusion of a finite atmosphere ahead of the shock, i.e., due to the abandonment of the strong-shock (infinite pressure ratio) assumption at that point. The Hugoniot relations give the shock density in terms of the shock pressure as

$$\rho = \frac{(\nu+1)\,P + (\nu-1)}{(\nu-1)\,P + (\nu+1)} = \frac{6\,P+1}{P+6} \text{ for } \gamma = 1.4 . \qquad (21)$$

For a strong shock ($P = \infty$) the density ratio is six ($\rho = 6$), but at two hundred atmos ($P = 200$) the ratio is only 5.83.

The strong shock solution is derived on the assumption that the atmosphere ahead of the shock wave has negligible effect. The effect, when non-negligible, is to raise the temperature through the shock to a higher value than that given by the strong shock solution, i.e., a finite shock is hotter than would be predicted by the "strong-shock" theory.

GAS VARIABLES AS A FUNCTION OF EULERIAN POSITION (λ)

The pressure, density, compression, and particle velocity are shown relative to their peak or shock values as functions of the Eulerian position (λ) in Fig. 7. The strong shock form dominates the first two sets, while the later ones show the characteristic positive phase followed by a longer, weaker negative phase and eventually by a return to near pre-shock values at the origin.

POSITIVE AND NEGATIVE PHASES VERSUS DISTANCE

The durations of the positive phases for pressure and particle velocity are shown in Fig. 8. Although these durations should approach the same value at large distances, they still differ by 7 percent at a distance of $\lambda = 3.0$ ($\Delta P_s = 0.09$). The figure indicates only the values for the point source solution.

The duration of the negative pressure phase (D_p^-), unlike that of the positive phase, is nearly independent of distance, and has an average value of 1.22. The negative durations suffer somewhat from loss of numerical significance at late times in the calculation.

TIME DEPENDENCE OF PRESSURE

In Fig. 9, the curves of pressure versus time at various distances are given in units of the peak overpressure and the positive duration in order to illustrate the change in the rate of decay behind the shock. At increasing

distances the drop in pressure is both relatively and absolutely slower since the positive phase duration is also increasing. Again, these curves are for the point-source solution.

An exponential form approximates the time dependence of the pressure pulse:

$$\frac{\Delta P}{\Delta P_s} = (1 - Z)e^{-\alpha Z} \tag{22}$$

Here Z is the time after shock arrival in units of positive duration, ΔP_s is the shock overpressure, and α is independent of Z. This form is satisfactory for overpressures less than one atmosphere ($\lambda > 0.74$), with the coefficient (α) specified by

$$\alpha = 1/2 + \Delta P_s, \quad \Delta P_s \leq 1 \tag{23}$$

For shock overpressures greater than one atmosphere the decay is not a simple exponential, since the early portion requires a larger α than the later part. Allowing the coefficient α to be a function of the time (Z), it may be approximated by

$$\alpha = 1/2 + \Delta P_s \left[1.1 - (.13 + .2\ \Delta P_s)Z\right] \tag{24}$$

for ΔP_s less than 3 atmos, and for overpressures from 3 up to 50 atmos by the form

$$\alpha = a + \frac{b}{1+eZ} \tag{25}$$

where

$$a = \begin{cases} -0.231 + 0.388\ \Delta P_s - 0.0332\ \Delta P_s^2 & \text{for } \Delta P_s \leq 10 \\ 0 & \text{for } \Delta P_s > 10 \end{cases}$$

$$b = \begin{cases} \Delta P_s(0.88 + 0.072\ \Delta P_s) & \text{for } \Delta P_s < 10 \\ \Delta P_s(1.67 - 0.011\ \Delta P_s) & \text{for } \Delta P_s \geq 10 \end{cases}$$

$$e = 8.71 + 0.1843\ \Delta P_s - 104/(\Delta P_s + 10)$$

The time dependence of the pressure in the negative phase may be approximated by the form

$$\Delta P = 14\ \Delta P_{-}\ \omega(1 - \omega)\epsilon^{-4\omega} \quad \text{for } 0.1 < \Delta P_s < 200 \tag{26}$$

where ΔP_{-} is the peak negative overpressure (see Fig. 10), and where ω is the time measured from the end of the positive phase in units of the negative phase duration (D_p^-). A more accurate fit would allow the exponent to decrease to zero as the shock strength goes to zero.

DYNAMIC PRESSURE VERSUS TIME

Of interest also is the form of the dynamic pressure ($Q = 1/2\ \rho u^2$). Time plots of this function appear in Fig. 11. These curves are also normalized, but with the positive duration of the particle velocity (D_u^+) (Fig. 8), and the peak value of the dynamic pressure (Q_s) (Fig. 3).

A similar exponential form approximates the dynamic pressure,

$$\frac{Q}{Q_s} = (1 - Z)^2\ \epsilon^{-\beta Z}\ . \tag{27}$$

where β is independent of the time (Z) for shocks of less than one atmos peak overpressure ($\Delta P_s < 1$). The coefficient β changes with the shock strength, however:

$$\beta = 0.75 + 3.2\ \Delta P_s, \quad \Delta P_s \leq 1\ . \tag{28}$$

Where the shock is stronger, a modification similar to that given in Eq. (25) for the overpressure is appropriate:

$$\beta = d + \frac{f}{1+gZ} \tag{29}$$

for

$$50 > \Delta P_s > 1\ ,$$

$$d = \begin{cases} -1.33\ \Delta P_s & \text{for } \Delta P_s \leq 3 \\ -5.6 + 0.63\ \Delta P_s & \text{for } 3 < \Delta P_s \leq 10 \\ 0 & \text{for } \Delta P_s > 10 \end{cases}$$

and $$f = 6.40\ \Delta P_s$$

$$g = 0.725\ \Delta P_s$$

These approximate forms agree with the numerical values of Q and ΔP in the positive phase to within 10 percent (and over most of the range to less than 2 percent) for values of ΔP_s less than ten atmos.

POSITIVE IMPULSE

The integrated positive overpressure (I_p^+) and the total positive drag pressure (I_u^+) decrease with distance from the blast source in the manner shown in Fig. 12.

$$I_p^+ = \int_0^{D_p^+} \Delta P(t)\ dt\ , \tag{30}$$

$$I_u^+ = \frac{1}{2} \int_0^{D_u^+} \rho u^2\ dt\ .$$

(Because of the units employed in this paper, I_u^+ does not become the usual dynamic impulse until it is multiplied by $\gamma = \frac{\rho_o C_o^2}{P_o}$)

Both of these impulses may be fitted by simple powers of the radial distance for shock overpressures less than two atmospheres:

$$I_p^+ = 0.043\ \lambda^{-1}\ , \quad \Delta P_s < 2 \tag{31}$$

$$I_u^+ = 0.004\ \lambda^{-2.7}$$

NEGATIVE IMPULSE

The negative overpressure impulse in the range below 20 atmos of peak overpressure can be expressed to within 5 percent by

$$I_p^- = \frac{1}{2}\ \Delta P_- D_p^-\ . \tag{32}$$

Since the duration of the negative pressure is constant at $D_p^- = 1.22$,

$$I_p^- = 0.61\ \Delta P_- \ . \tag{33}$$

For distances greater that $\lambda = 0.5$ the negative peak overpressure approaches zero inversely as the distance

$$\Delta P_- = -\ 0.086\ \lambda^{-1} \quad , \lambda\ > 0.5\ , \tag{34}$$

and the negative pressure impulse goes approximately like

$$I_p^- = 0.052\ \ \lambda^{-1} \quad , \lambda\ > 0.5\ \ . \tag{35}$$

SPECIAL FEATURES OF THE ISOTHERMAL SPHERE PROBLEMS

In the gas dynamics resulting from the release of an initially static high-pressure sphere, an inward moving shock forms behind the rarefaction wave that first runs in from the surface of the sphere. This inward-directed shock was predicted by Wecken[7] and discussed by McFadden[8], Shardin[9] and others[4]. It does not acquire a net inward velocity until the rarefaction has reached the center, but after that it moves in and reflects at the origin, and then races outward to eventually overtake the main shock.

This second shock grows from zero strength to presumably an infinite pressure ratio at the origin. On reflection, this shock moves outward, decaying in strength about as the inverse first power of its distance from the origin. The general expansion and outward motion of the gas behind the main shock is responsible for this apparently modest decay rate.

When this second shock encounters the outer surface of the gas that was initially inside the sphere, a transmitted shock continues out and a reflected shock is sent inward. The transmitted shock overtakes the main shock and increases it by as much as 20%. Progressively weaker shocks

follow from the reflections at the interface and again at the origin. This repeated shocking of the gas near the origin changes the temperature profile at later times from its initial isothermal nature to nearer the point-source distribution which is characterized by a high central temperature falling off rapidly with radius.

Some detail is lost in the vicinity of the origin since the shocks are always spread over a number of mesh points. In one case the problem was re-run with mesh sizes about one fourth the original size, and the inward-moving shock showed some appreciable discrepancy near the origin. However, this discrepancy may be attributed mainly to the difficulty in identifying the shock when the rounding is comparable to the shock radius. After reflection the difference vanishes again in spite of the quite different histories near the center.

IV. CONCLUSIONS

POINT SOURCE SOLUTION

At increasing distances from a finite but sudden source of energy, the resulting blast wave will appear more and more like that from a point source. The blast resulting from an initial isothermal sphere of gas at rest will assume the general shape and values of the point source solution (to within 10 percent) after the shock wave has engulfed a mass of air 10 times the initial mass of the sphere. Prior to this, the shock strength is less than that of the point source shock, and the inward-traveling rarefaction has not reached the center.

A point source should leave a higher temperature and consequently a larger percentage of energy near the origin. This energy, no longer available to the shock wave, should effect a reduction in the shock radius (for a given overpressure). However, no appreciable difference in the low-end of the shock overpressure-radius relation appears on comparing the point source and isothermal sphere solutions. In fact, perhaps due to multiple shocking of the inner regions in the isothermal sphere problems, the distribution of residual energies (per unit volume) and pressures are nearly identical around the origin at a time when the shock has progressed to 6 or 7 times the initial radius. Although temperatures will remain different, since the point source has an infinite temperature at the origin (and zero density), the average temperature (or density) of that gas initially inside the isothermal sphere approaches (within 10 percent) the average temperature for a corresponding mass around the point source.

For a source of considerable initial mass, the peak pressure may become quite small before the shock has engulfed a mass of gas 10 times larger, and the blast wave may, therefore, remain quite different from the point source solution throughout regions of interest. Such is the case to some extent with high explosives where initial charge shapes will influence the blast wave at all significant pressures. It is true to an even greater extent in the spherical equivalent of a shock-tube type of blast, where a gas at high pressure but at normal temperature is suddenly released, as in the normal temperature isobaric sphere problem (dotted curve Fig. 1) described in Section I.

APPLICATION TO BLAST IN AIR

The ideal gas assumption is reasonably valid in air for shock pressures less than 10 atmos. Above that the gamma in the expression for the internal

energy (Eq. 7) ranges down to as low as 1.133 and up to the mono-atomic value of 1.667.

But since the mass of gas which has experienced shocks stronger than 10 atmos is a small part (5 percent) of the engulfed mass by the time the shock overpressure is down to 1 atmos, the blast wave for constant gamma should be reasonably correct for air at most interesting shock pressures.

In the case of shock wave problems involving only one space variable, the artificial viscosity technique for numerical integration appears to be very satisfactory over large ranges of pressure and entropy change. Unfortunately, it cannot be expected to yield details of a shock wave impinging on a singular point such as the origin in spherical or cylindrical geometry, since the nature of this method is such as to spread the shock front over a number of grid points.

ACKNOWLEDGMENTS

The persons participating in and aiding the work reported on here are too numerous to list; however, at the risk of slighting many, I mention a few: R. Latter gave some critical attention to the formulation of the problem. Ruth Anne Engvall, I. Greenwald and other mathematicians performed much of the coding and numerical work. Miss Engvall also supervised much of the analysis of results and the preparation of curves. In addition, the author enjoyed frequent helpful discussions with other RAND personnel and consultants.

This work was accomplished with the aid of both Air Force and Atomic Energy Commission funds.

REFERENCES

1. Shock Hydrodynamics and Blast Waves, Los Alamos Scientific Laboratory, Report AECD-2860 (1944).

2. Lax, P. D., Communications on Pure and Applied Mathematics, Inst. of Mathematical Sciences, New York University, Vol. VII, pp. 159-193 (1954).

3. von Neumann, J., and R. D. Richtmyer, J. Appl. Phys., 21, 232 (1950).

4. Walton, T. S., Phys. Rev. 87, 910(A) (1952).

5. Latter, R., Unpublished, The RAND Corporation.

6. Du Fort, E. C., and S. P. Frankel, Mathematical Tables and Other Aids to Computation, Vol. VII, pp. 135 (1953).

7. Weeken, F., Expansion Einer Gaskugel Hohen Druckes, Z. Angew Math. Mech. 30, 270 (1950).

8. McFadden, J. A., J. Appl. Phys., 23, 1269 (1952).

9. Schardin, H., Measurement of Spherical Shock Waves, Communications on Pure and Applied Mathematics, Inst. of Mathematical Sciences, New York University, Vol. VII, p.223 (1954).

FIGURE CAPTIONS

Fig. 1 - Radial dependence of the peak or shock overpressure. The solid curve represents the point source solution. The dashed curves represent the results from two different initial isothermal spheres, one at 2000 atmos and the other at 121 atmos, both spheres were hot with equal density inside and out. The dotted curve represents the resulting shock overpressure from an initially cold isobaric sphere with temperature equal inside and out. The pressures are in atmos and the distances in units of $(E_{tot}/P_o)^{1/3}$.

Fig. 2 - Particle velocity or Mach number at the shock as a function of shock radius for the point source solution. Velocity is in units of the pre-shock sonic velocity and the radius is in units of $(E_{tot}/P_o)^{1/3}$.

Fig. 3 - Peak or shock dynamic pressure ($Q = 1/2\ \rho u^2$) versus shock radius for the point source solution. The dynamic pressure is in atmos and the radius in units of $(E_{tot}/P_o)^{1/3}$.

Fig. 4 - Pressure in atmos as a function of the Lagrange or mass position for the point-source solution at times indicated. The position is in arbitrary units of $(E_{tot}/P_o)^{1/3}/1627.2$, and the time is in units of $(E_{tot}/P_o)^{1/3}/C_o$ when C_o is the preshock sonic velocity.

Fig. 5 - Particle velocity in units of preshock sonic velocity as a function of Lagrange or mass position for the point-source solution at the times indicated. The position is in units of $(E_{tot}/P_o)^{1/3}/1627.2$, and the time is in units of $(E_{tot}/P_o)^{1/3}/C_o$.

Fig. 6 - Density in units of preshock density as a function of Lagrange or mass position for the point-source solution at the times indicated. The position is in units of $(E_{tot}/P_o)^{1/3}/c_o$.

Fig. 7 - Hydrodynamic quantities in units of their peak values as a function of Eulerian or space position at the times indicated. The radius is in units of $(E_{tot}/P_o)^{1/3}$. The solid curves represent overpressure $(\Delta P/\Delta P_s)$, the long dash curves represent particle velocity (u/u_s), the dot-dash curves represent density (ρ/ρ_s), and the short dash curves represent compression $\left[(\rho-1)/(\rho_s-1)\right]$. The shock values of the overpressure (ΔP_s) for these times are 121.5, 20.10, 2.03, 1.01, 0.338, 0.0701 ordered on increasing time. For the particle velocity the peak values are 8.49, 3.37, 0.873, 0.524, 0.216, 0.0525, and for the density the peak values are 5.66, 4.68, 2.135, 1.625, 1.228, 1.0508.

Fig. 8 - Duration of positive phase for pressure (D_p^+) and particle velocity (D_u^+) versus distance (Eulerian) where time is in units of $(E_{tot}/P_o)^{1/3}/c_o$ and distance is in units of $(E_{tot}/P_o)^{1/3}$.

Fig. 9 - Pressure as a function of time where the pressure is in units of the peak pressure (ΔP_s)(Fig. 1) and the time $(\bar{t}_p)$ is in units of the positive duration (D_p^+) (Fig. 8). The numbers indicate the corresponding peak overpressures (ΔP_s).

Fig. 10 - Peak negative overpressure in atmos as a function of radial distance in units of $(E_{tot}/P_o)^{1/3}$.

Fig. 11 - Dynamic pressure ($Q = 1/2\ \rho u^2$) as a function of time where the pressure is in units of the peak dynamic pressure (Q_s) (Fig. 3), and the time is in units of the positive duration of the velocity (D_u^+) (Fig. 8). The numbers indicate the corresponding peak overpressures (ΔP_s). This rapid decrease in effective pulse duration with increasing peak overpressure has the effect of making the higher dynamic impulses much the sharpest.

Fig. 12 - The radial dependence of the positive pressure impulse (I_p^+) the negative pressure impulse (I_p^-), and the positive dynamic impulse I_Q^+ in units of atmospheres (where time is in the dimensionless units $(E_{tot}/P_o)^{1/3}/C_o$) the radial distance is in units of $(E_{tot}/P_o)^{1/3}$.

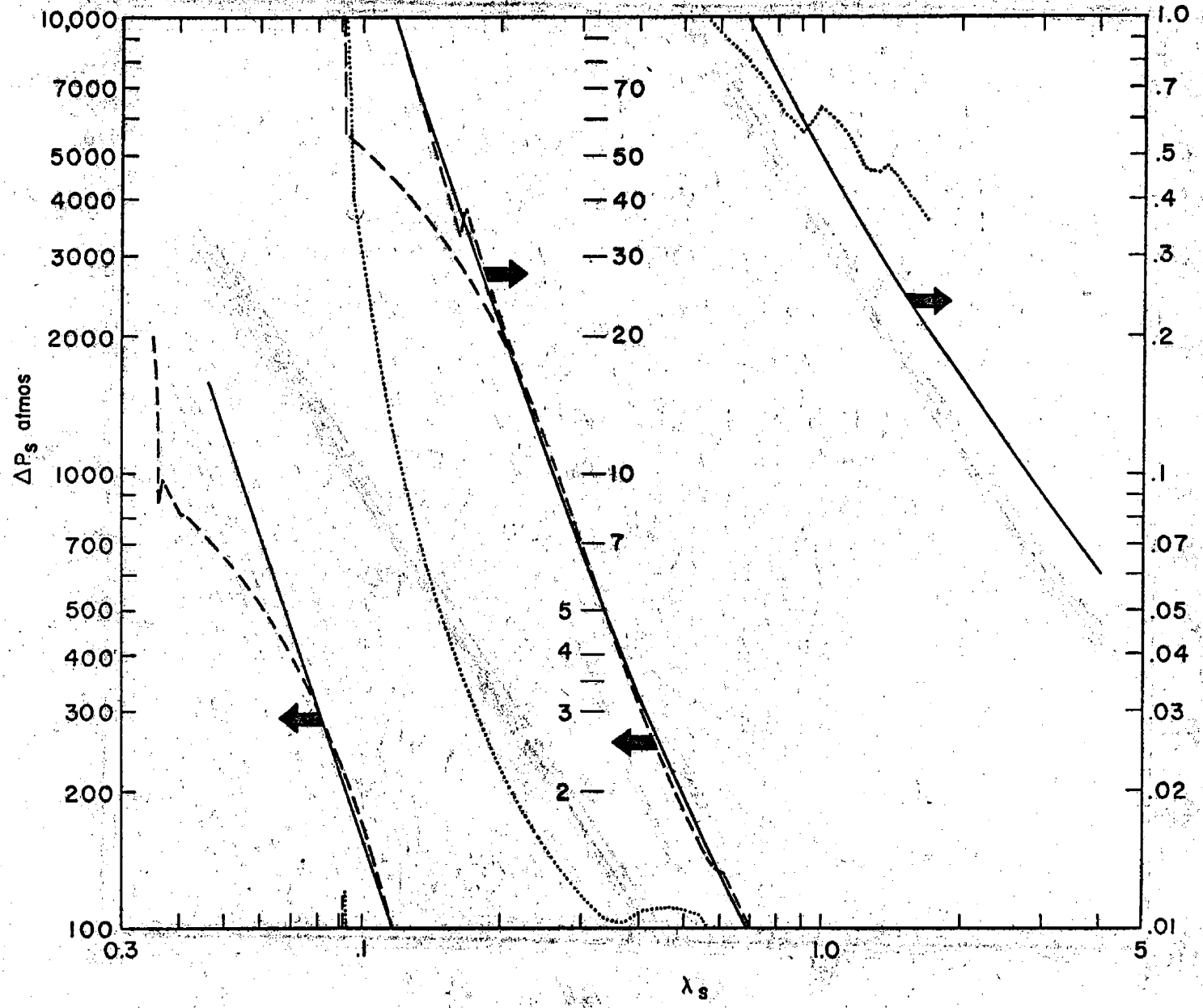
10,000
7000
5000
4000
3000
2000
1000
700
500
400
300
200
100
ΔP_s atmos
70
50
40
30
20
10
7
5
4
3
2
1.0
.7
.5
.4
.3
.2
.1
.07
.05
.04
.03
.02
.01
0.3
.1
1.0
5
λ_s

Figure 1

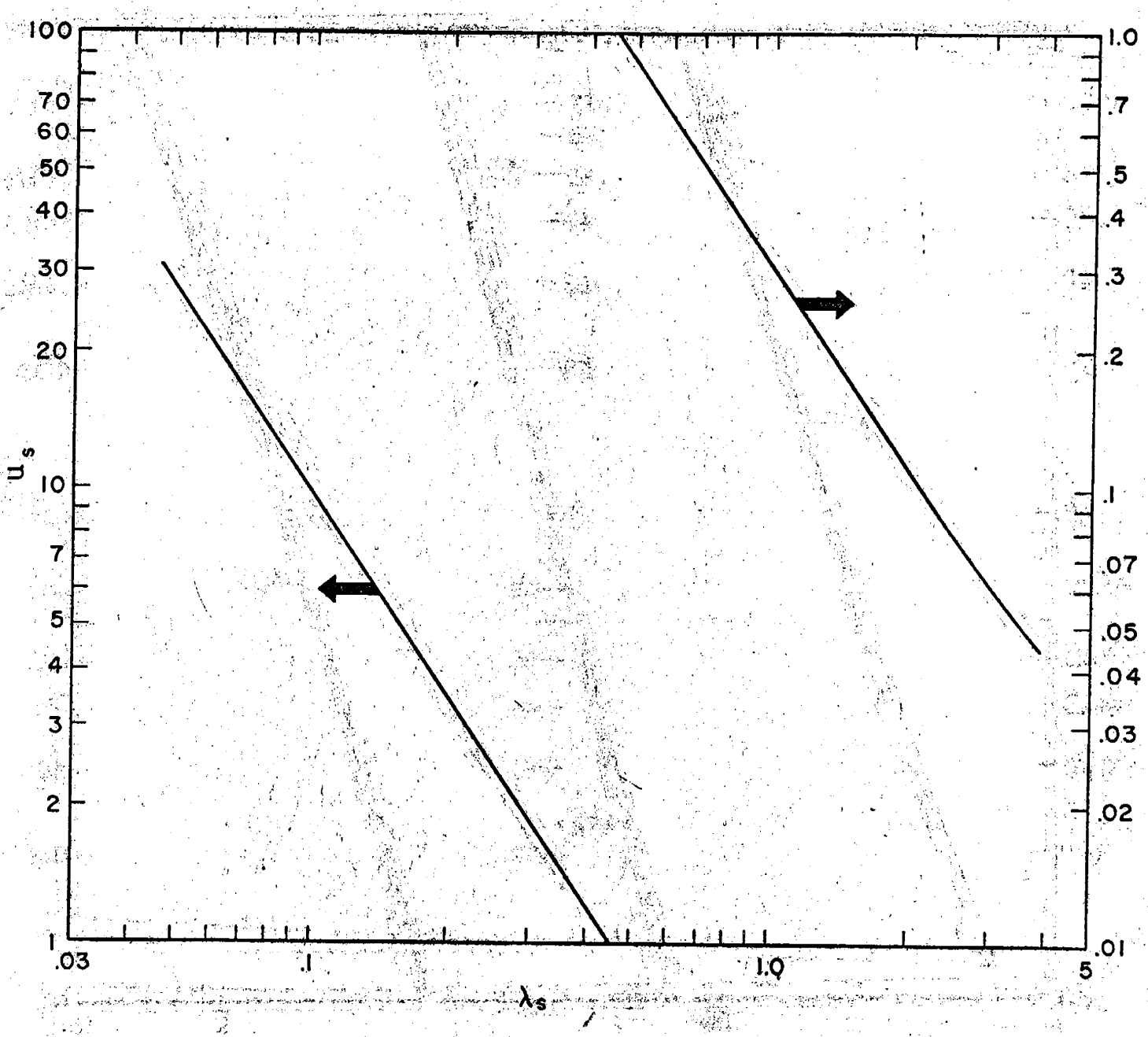
100
70
60
50
40
30
20
10
7
5
4
3
2
1
n_s
.03
.1
1.0
5
λ_s
1.0
.7
.5
.4
.3
.2
.1
.07
.05
.04
.03
.02
.01

Figure 2

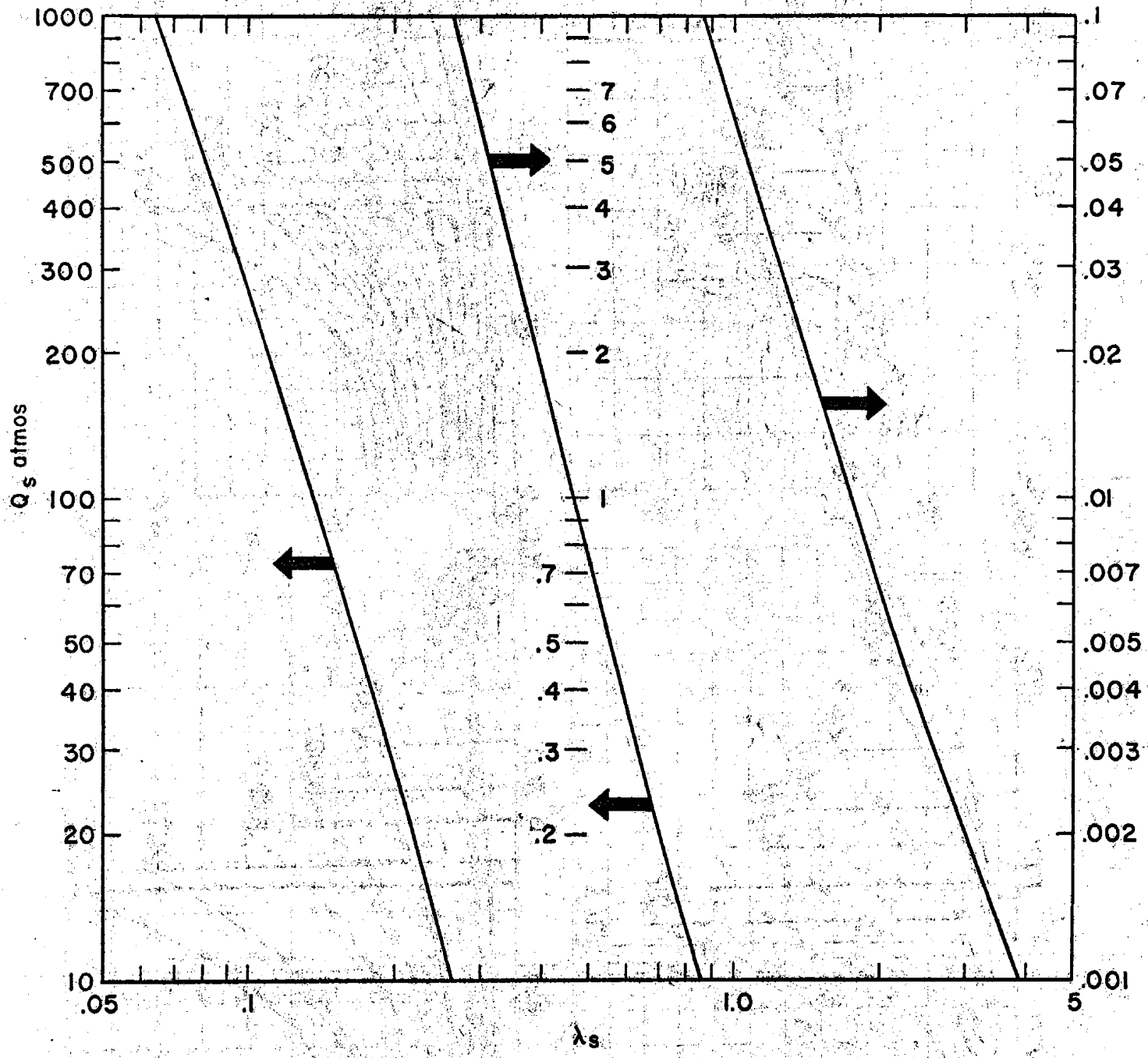
1000
700
500
400
300
200
100
70
50
40
30
20
10
Q_s atmos
.1
.07
.05
.04
.03
.02
.01
.007
.005
.004
.003
.002
.001
7
6
5
4
3
2
1
.7
.5
.4
.3
.2
.05
.1
1.0
5
λ_s

Figure 3

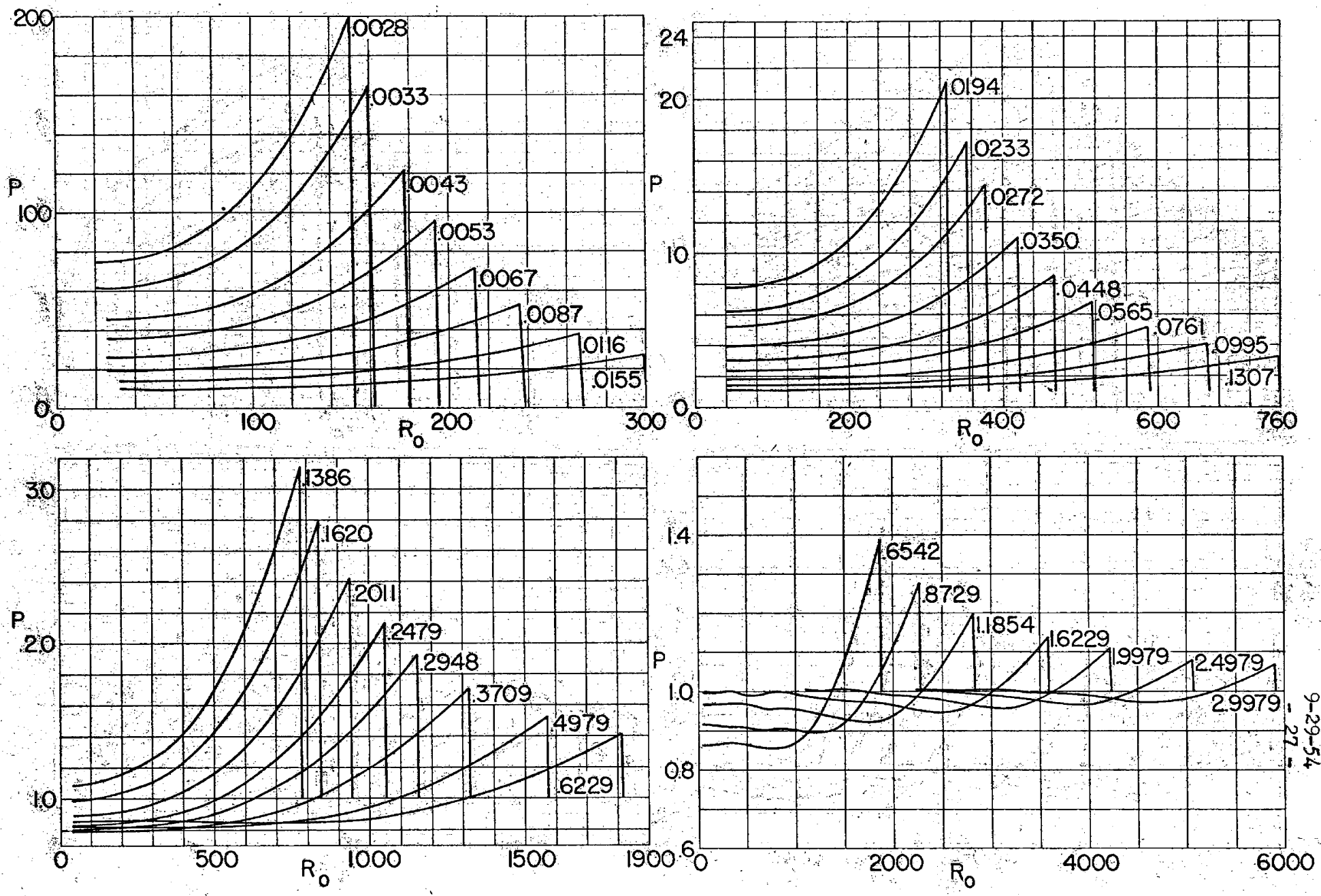
200
P
100
0
0
100
200
300
R_o
.0028
.0033
.0043
.0053
.0067
.0087
.0116
.0155
24
20
10
0
0
200
400
600
760
R_o
.0194
.0233
.0272
.0350
.0448
.0565
.0761
.0995
.1307
30
2.0
1.0
0
500
1000
1500
1900
R_o
.1386
.1620
.2011
.2479
.2948
.3709
.4979
.6229
1.4
1.0
0.8
0.6
0
2000
4000
6000
R_o
.6542
.8729
1.1854
1.6229
1.9979
2.4979
2.9979

Figure 4

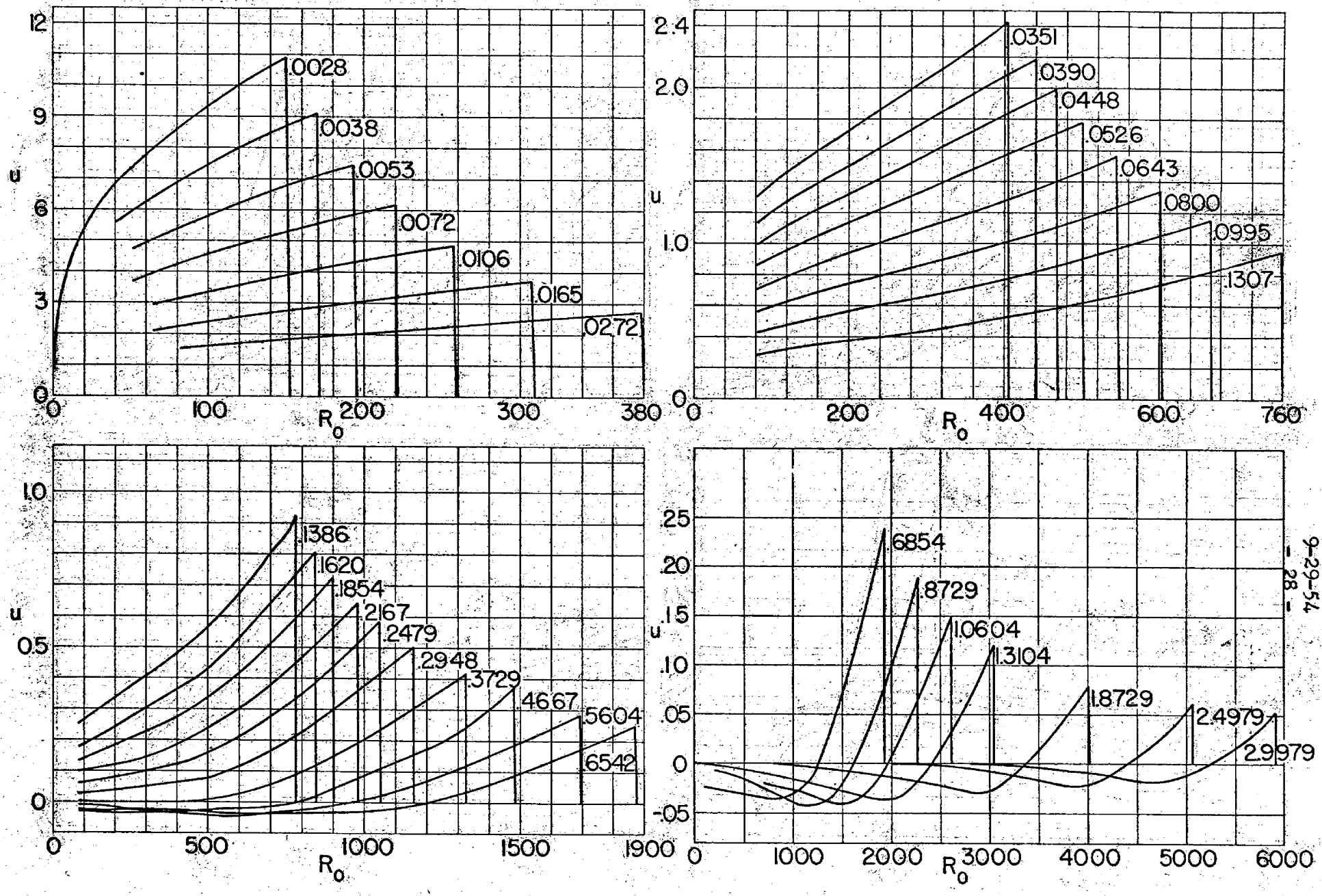
u
R_0
.0028
.0038
.0053
.0072
.0106
.0165
.0272
.0351
.0390
.0448
.0526
.0643
.0800
.0995
.1307
.1386
.1620
.1854
.2167
.2479
.2948
.3729
.4667
.5604
.6542
.6854
.8729
1.0604
1.3104
1.8729
2.4979
2.9979

Figure 5

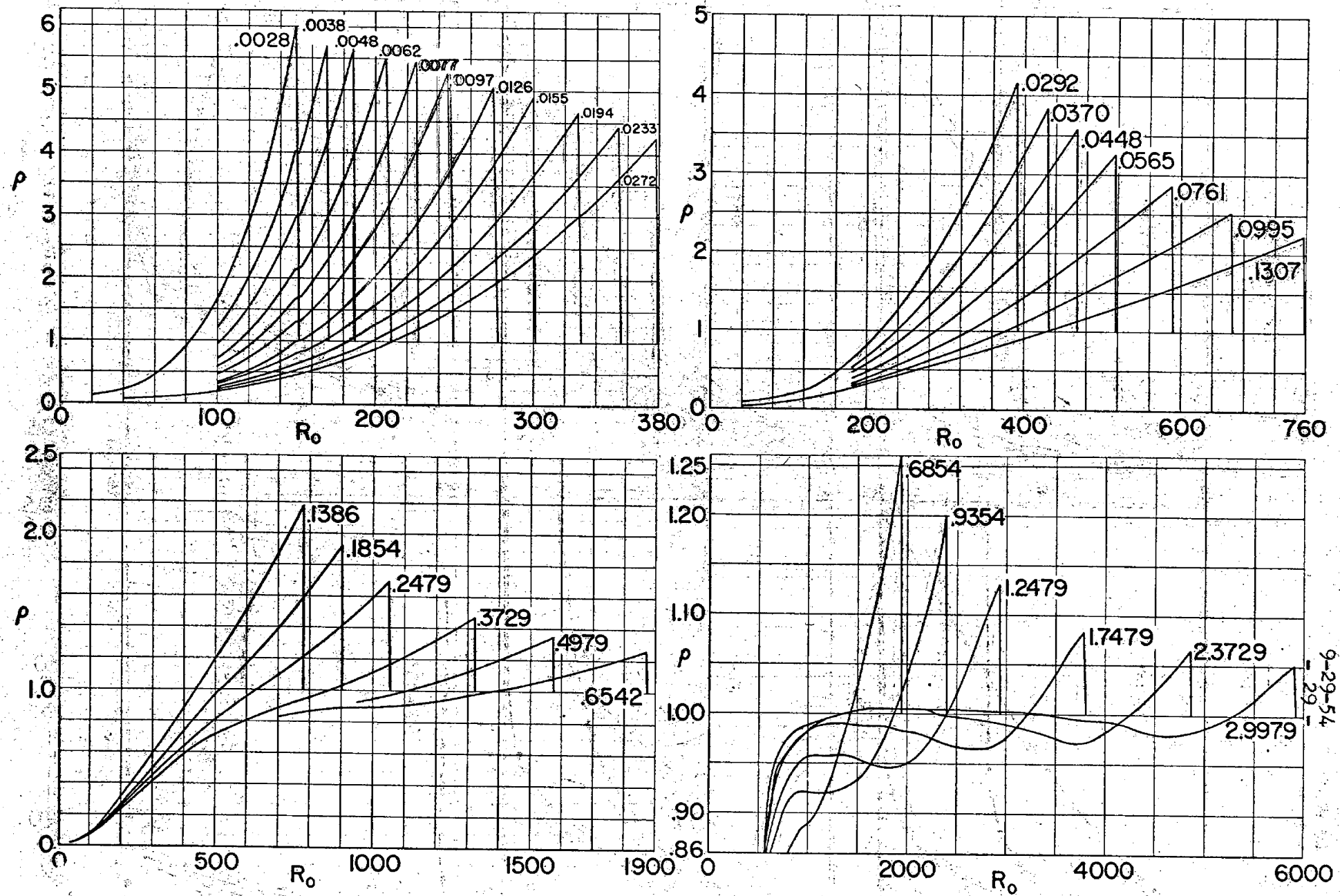
ρ
R₀
.0028
.0038
.0048
.0062
.0077
.0097
.0126
.0155
.0194
.0233
.0272
.0292
.0370
.0448
.0565
.0761
.0995
.1307
.1386
.1854
.2479
.3729
.4979
.6542
.6854
.9354
1.2479
1.7479
2.3729
2.9979

Figure 6

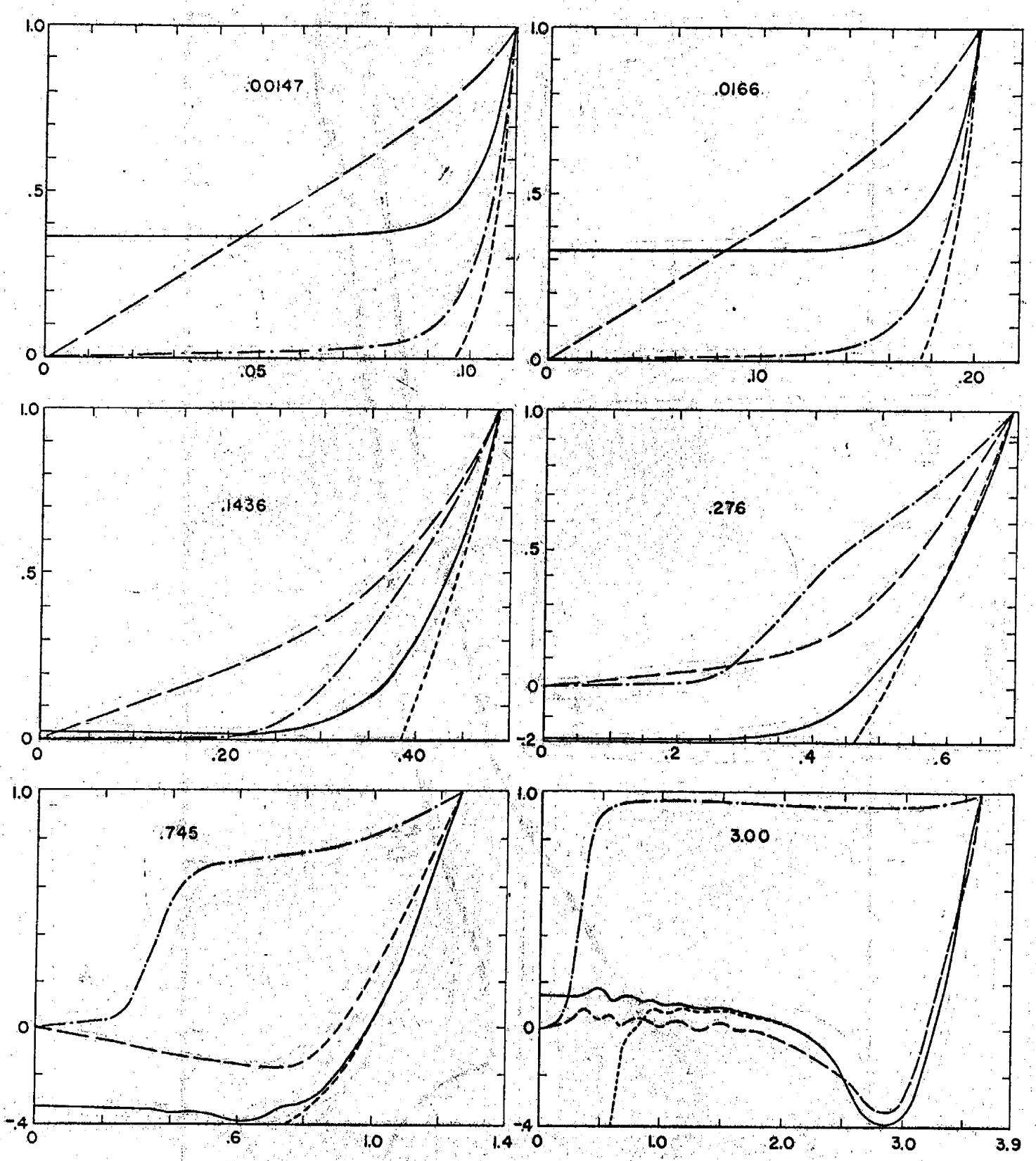

Figure 7

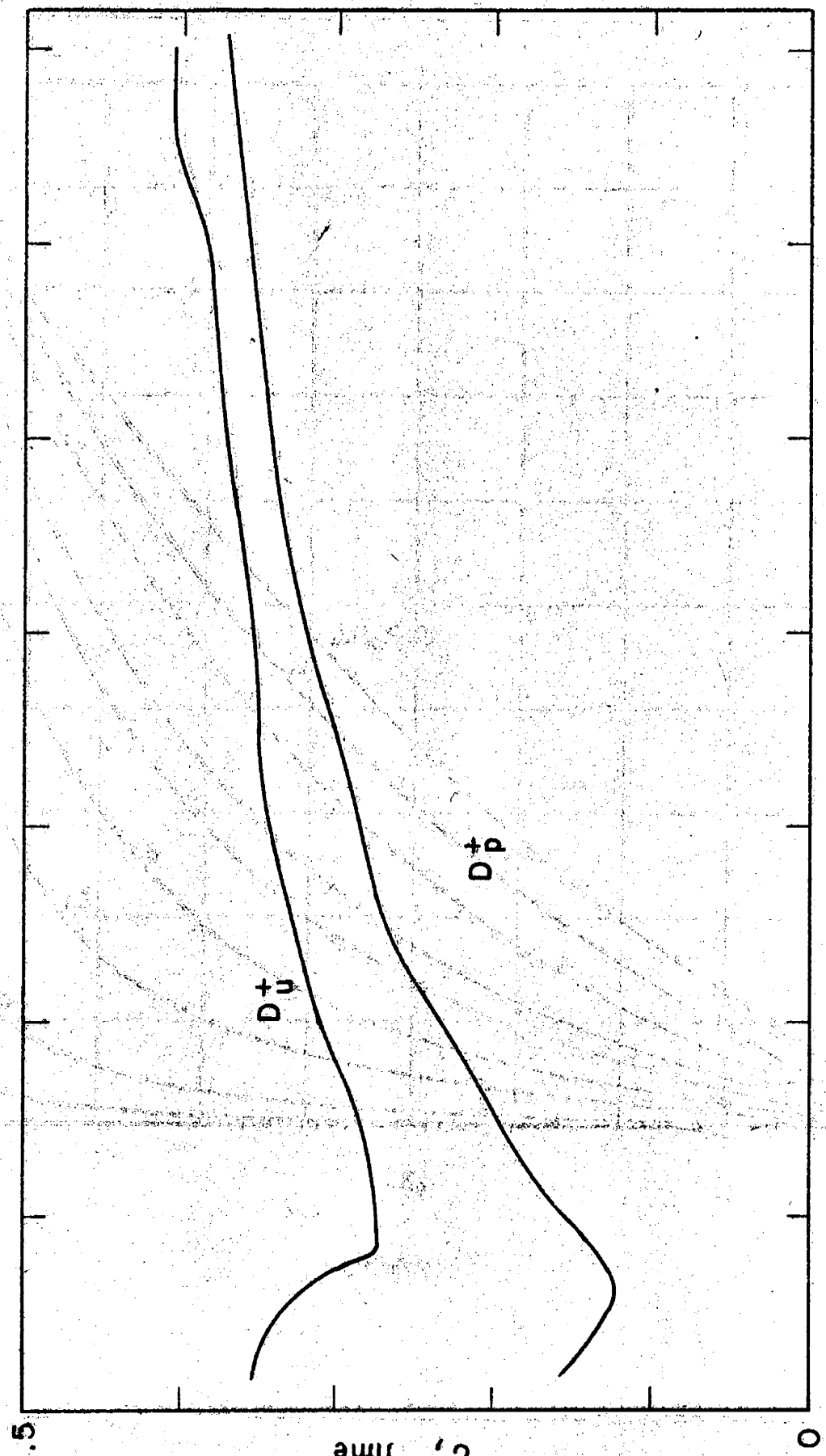

Figure 8

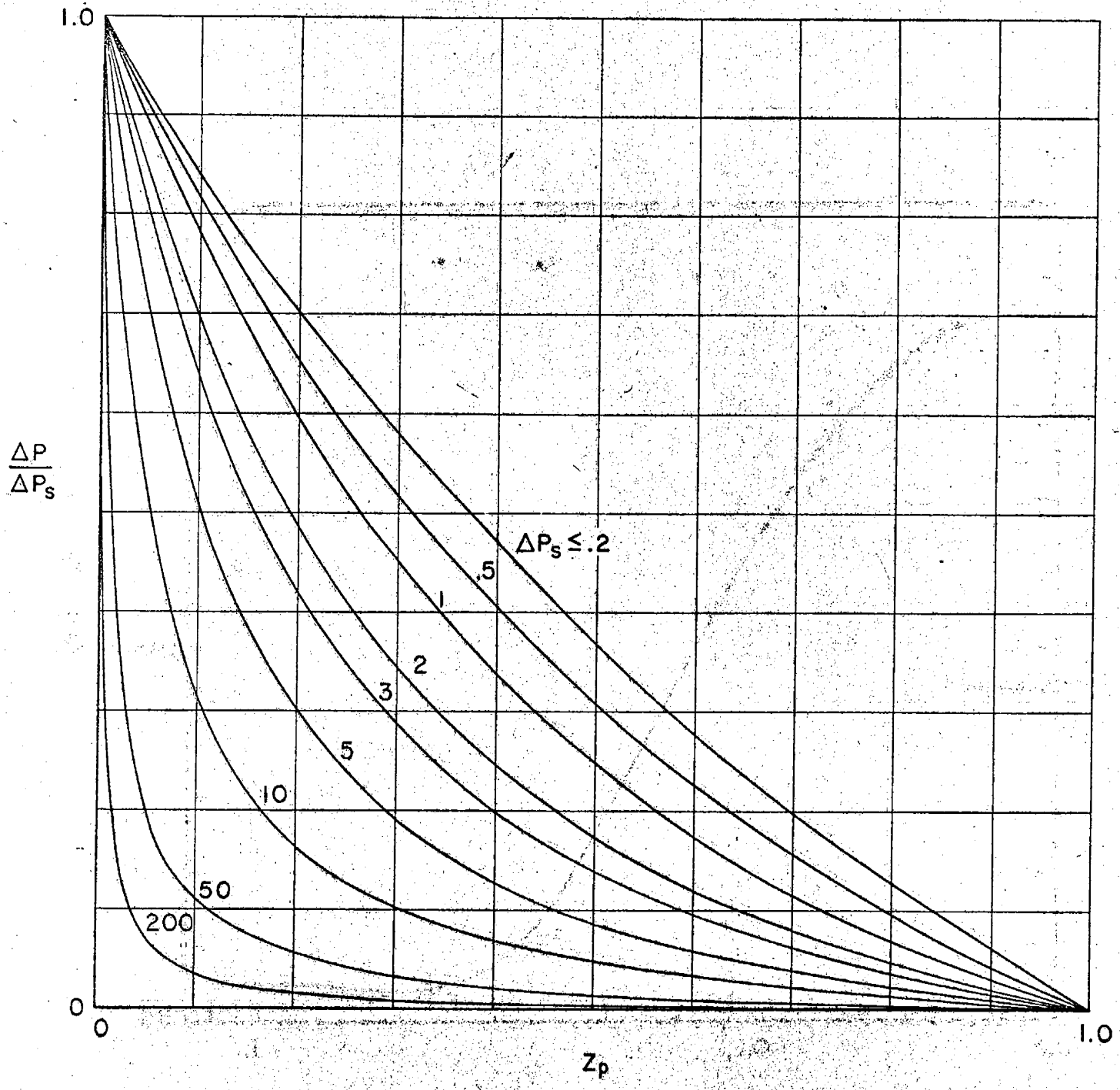

Figure 9

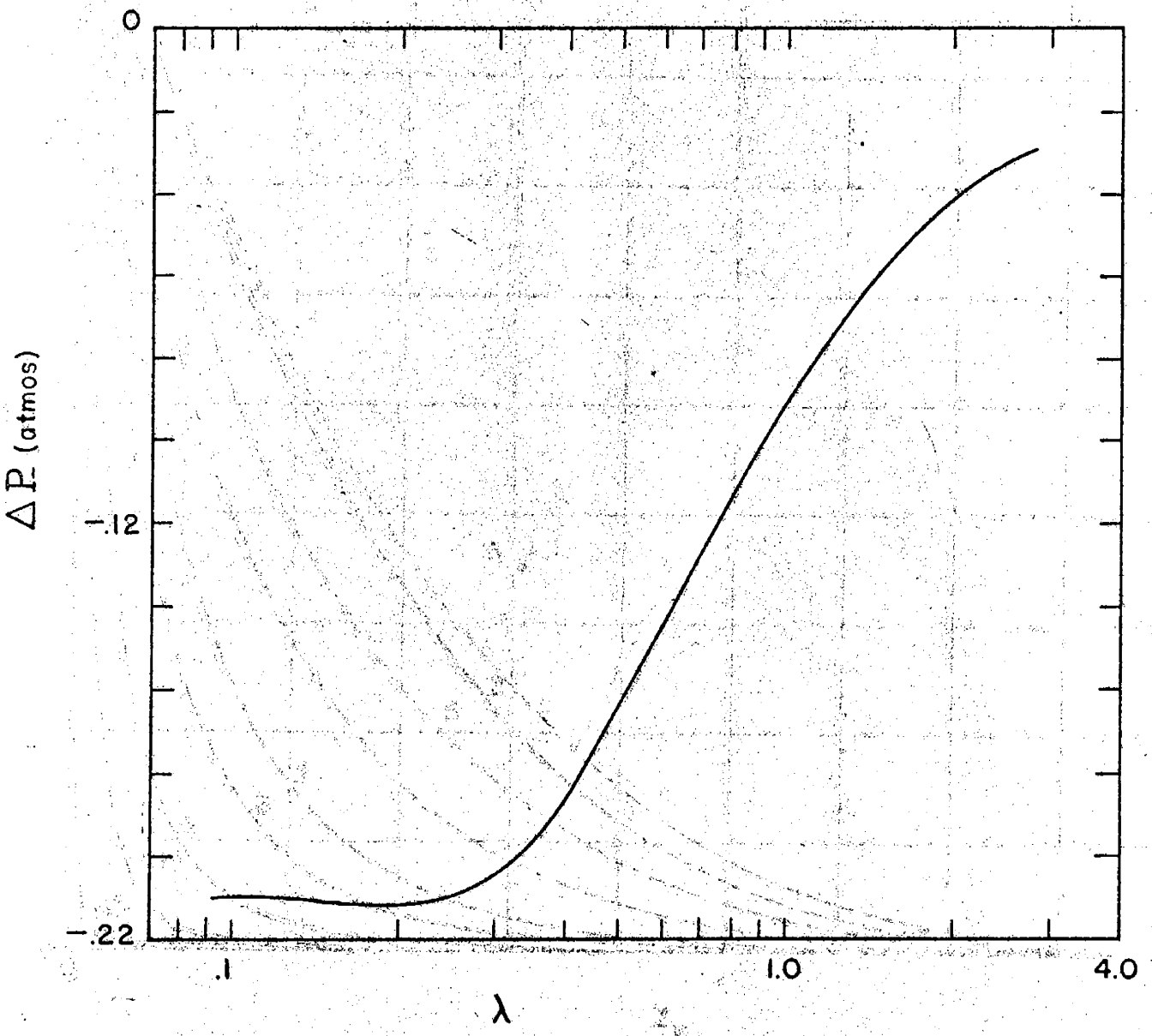

Figure 10

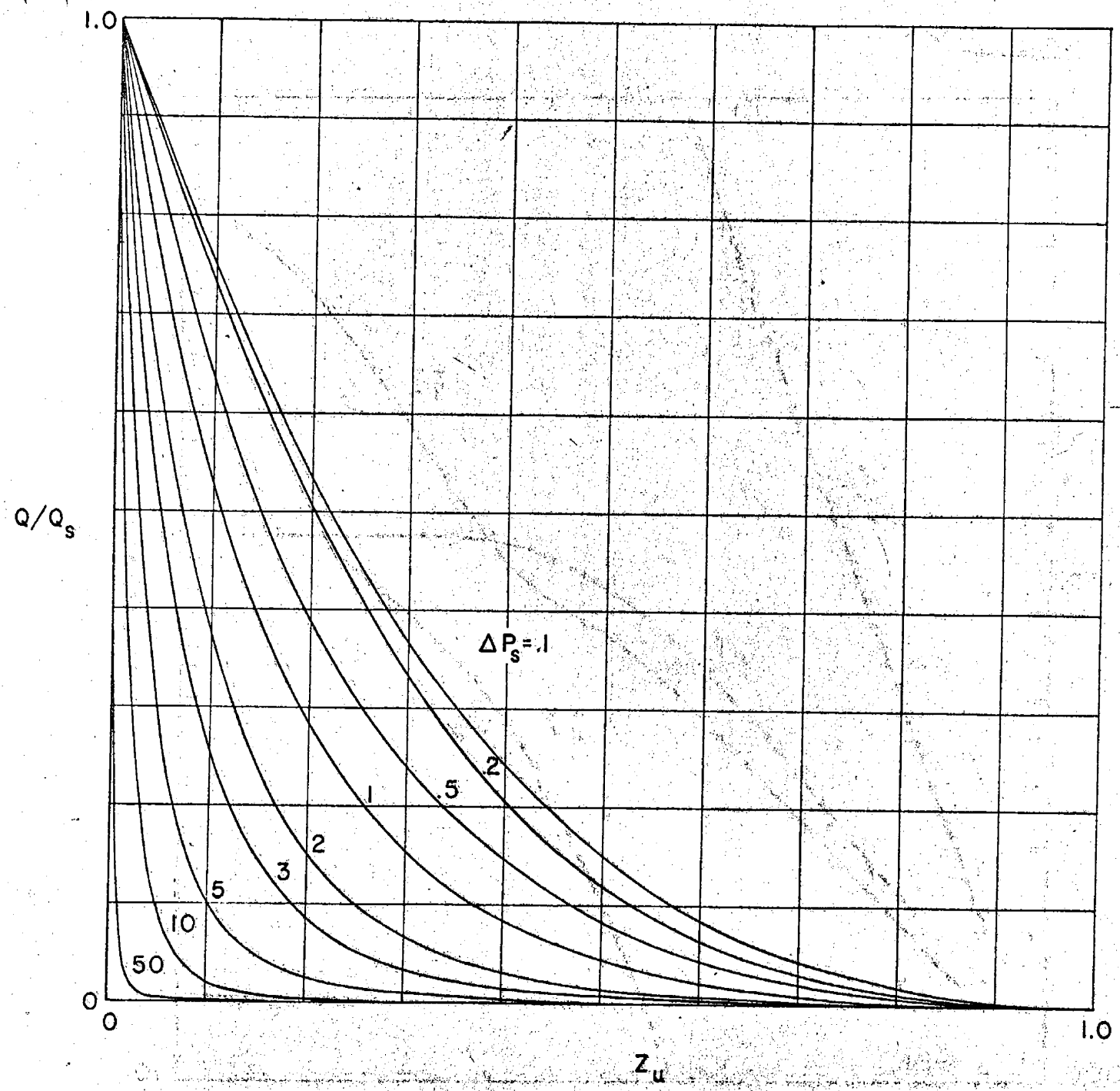

Figure 11

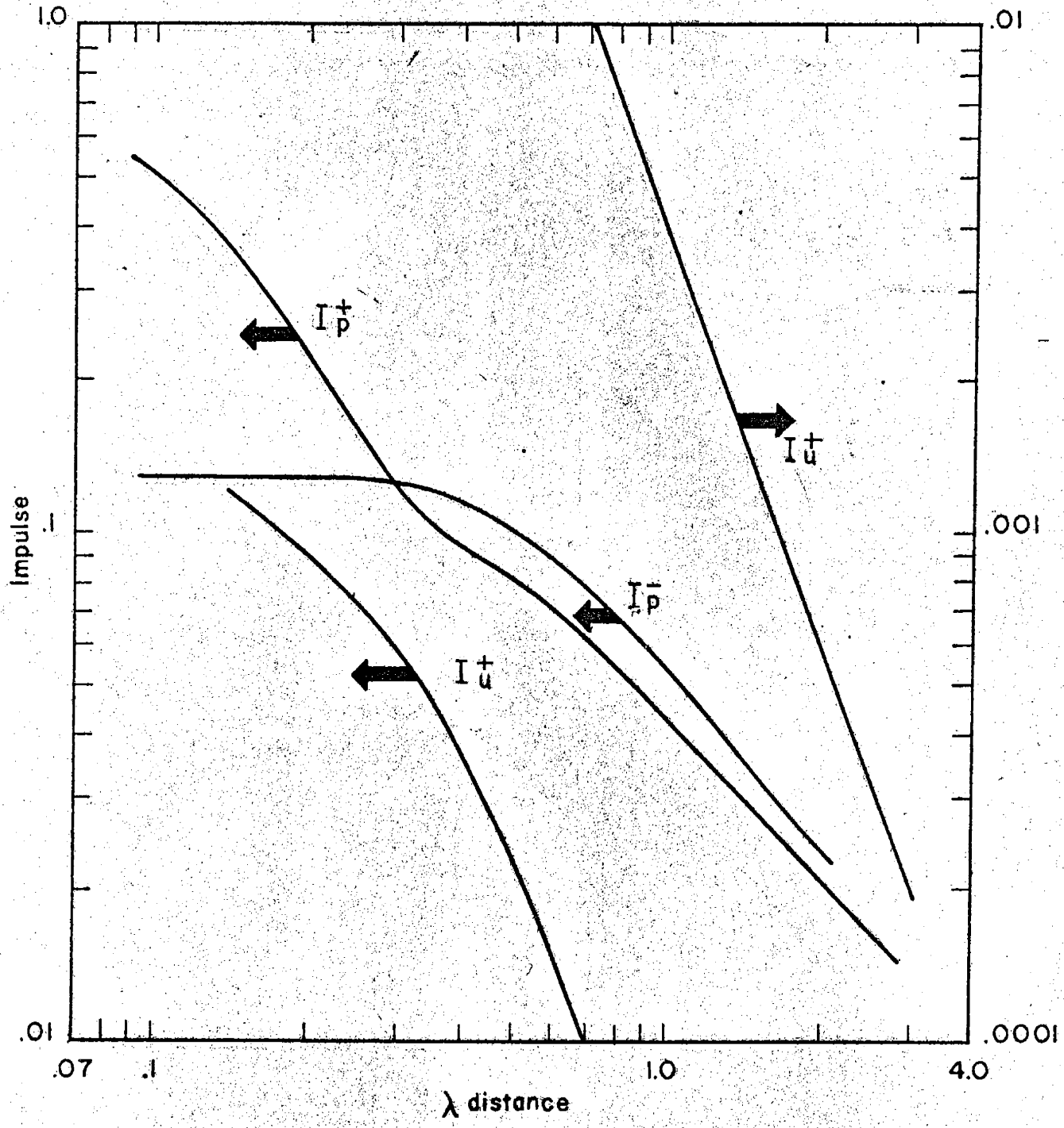

Figure 12